Preprints of the 23rd IFAC World Congress
Busan, Republic of Korea, August 23-28, 2026

Temporal Logic-Based Coverage and Path Planning for Unmanned Aerial–Ground Vehicle Systems ⋆

Shiheng Zhang *† **Yangrui Zhang** *† **Shaowen Miao** * **Yiding Ji** *

* *Robotics and Autonomous Systems Thrust of Systems Hub, The Hong Kong University of Science and Technology (Guangzhou), Guangzhou 511453, China (e-mail: {szhang593, yzhang112, smiao585}@connect.hkust-gz.edu.cn, jiyiding@hkust-gz.edu.cn).*

Abstract:
This paper addresses the cooperative coordination of unmanned aerial vehicles (UAVs) and unmanned ground vehicles (UGVs) in complex environments under formal task specifications. A two-layer control framework is developed, where UAVs perform coverage and monitoring tasks as a perception layer, while UGVs execute ground-level path planning with obstacle avoidance. The framework leverages Spatial Aggregation Signal Temporal Logic (SaSTL) to formally specify both spatial and temporal behaviors, which allows real-time monitoring of collective task execution through computing robustness measures of properly defined SaSTL formulas. To ensure feasibility, an Attractive Potential Field (APF) approach incorporates the "Eventually" specifications into the path planning objectives, while time-varying Control Barrier Functions (CBFs) enforce "Always" safety constraints via a quadratic programming (QP) solver. The proposed framework ensures optimal coverage and collision-free planning via task monitoring, whose performance is validated through substantial numerical simulations over several scenarios.

Keywords: Signal temporal logic, formal methods, multi-agent systems, coverage control, path planning, real-time monitoring

1. INTRODUCTION

Multi-agent systems (MASs), particularly heterogeneous teams comprising quadrotor unmanned aerial vehicles (UAVs) and unmanned ground vehicles (UGVs), have garnered attention for their potential in complex, large-scale missions Lizzio et al. (2022); Zhang et al. (2024); Zhang and Ji (2025b,a). By leveraging the capabilities of different agents, MASs achieve superior scalability, flexibility and reliability unattainable by individual agents. Typical application includes autonomous environmental monitoring, infrastructure inspection, and search and rescue after disasters Zhong and Cassandras (2011). In these scenarios, a core task for the agents is cooperative coverage control, which involves the strategic distribution of sensor-equipped agents to surveil a target environment.

Despite their promise, real-world deployment of MASs is often hindered by irregular obstacles and dynamic terrains. These uncertainties present two critical challenges: (1) limited local sensing capabilities that restrict an agent's perception of global target locations Wang et al. (2025), and (2) the risk of mission failure due to collisions or entry into restricted zones Palacios-Gasós et al. (2017). To address the issues, a hierarchical decomposition is often employed, where UAVs with high maneuverability and wide sensing ranges serve as an aerial perception layer, while UGVs handle ground navigation and precise target interaction. A representative application is post-earthquake rescue Yousefi et al. (2024), where UAVs perform aerial perception to identify targets and obstacles, while UGVs transport supplies to designated sites. The hierarchical control paradigm, where complex tasks are decomposed into multiple coordinated levels, requires formal specifications Zhang et al. (2026). Signal temporal logic (STL) Maler and Nickovic (2004) provides a powerful framework for encoding temporal requirements, but not for spatial reasoning. To bridge this gap, this paper leverages Spatial Aggregation Signal Temporal Logic (SaSTL), which extends STL with spatial operators Zhao et al. (2025). Originated for smart city modeling Ma et al. (2021), SaSTL is uniquely suited for MASs, as it formally defines tasks involving collective spatial configuration.

However, path planning through direct embedding of temporal logic formulas into quadratic programming (QP) often leads to computation burden and poor scalability Belta and Sadraddini (2019). While integrating Control Barrier Functions (CBFs) with STL has shown promise for real-time safety enforcement Lindemann and Dimarogonas (2019), existing methods are often overly conservative when handling multiple specifications. An alternative approach incorporates STL robustness into the optimal control objectives through smooth approximations and leverages gradient-based optimization Haghighi et al. (2019).

Motivated by these considerations, we propose a hierarchical perception-planning framework supported by spatio-

⋆ This work is supported by National Natural Science Foundation of China grants 62303389 and 62373289; Guangdong Province Scientific Research Platform and Project Scheme grant 2024KTSCX039; Youth Talent Support Program of Guangdong Association for Science and Technology grant SKXRC2025463 and Guangdong Provincial Key Lab of Integrated Communication, Sensing and Computation for Ubiquitous Internet of Things (No.2023B1212010007).
⋆*† Contributed equally; Corresponding author: Yiding Ji.

©2026 the authors. Accepted by IFAC for publication under a Creative Commons Licence CC-BY-NC-ND

temporal monitoring with SaSTL formulas. Adopting a "sense-then-act" coordination strategy, the framework exploits the complementary capabilities of heterogeneous agents: UAVs act as a perception layer to explore the environment, monitor spatial distributions and obstacles, and provide environmental constraints for the safe planning of UGVs through a sequential information flow. Different from conventional approaches focusing on trajectories of individual agents, our method utilizes SaSTL to formalize and monitor collective spatial aggregation requirements of heterogeneous MASs in real time, capturing both spatial configurations and temporal evolution without requiring extensive auxiliary variables as in standard STL. Furthermore, SaSTL specifications are decomposed into *Eventually* and *Always* fragments for collision-free UGV planning, where the former is incorporated into the objective function through an APF, and the latter is encoded as time-varying CBF constraints within a QP framework.

2. SYSTEM MODELING AND PRELIMINARIES

2.1 System Model of UAV–UGV Systems

Consider a three-dimensional environment $\mathcal{K} \subset \mathbb{R}^3$ containing signal sources $\mathcal{S}$ and obstacles $\mathcal{O}$. Let $\mathcal{Q} \subset \mathbb{R}^2$ denote the ground projection of $\mathcal{K}$. Each obstacle $i \in \mathcal{O}$ is represented on $\mathcal{Q}$ by a circular region $\mathcal{C}_i^o(x_i^o, r_o)$ with center x_i^o and radius r_o. The environmental information is described by the spatial density function

$$\phi(q) = \sum\nolimits_{i\in\mathcal{S}} g_i^s(q, \sigma_i, x_i^s), \tag{1}$$

where $g_i^s(\cdot)$ is a Gaussian function centered at x_i^s with σ_i^2.

We consider a heterogeneous multi-agent system composed of n UAVs and UGVs, denoted by $\mathcal{V}$ and $\mathcal{R}$, respectively. UAVs move in $\mathcal{K}$, while UGVs operate on $\mathcal{Q}$. Their projected positions are denoted by $\boldsymbol{x}^a(t) \in \mathbb{R}^{2\times n}$ and $\boldsymbol{x}^b(t) \in \mathbb{R}^{2\times n}$. All UAVs are assumed to fly at the same altitude, and obstacle avoidance is not considered in the coverage layer. The dynamics of both UAVs and UGVs are modeled as first-order integrators:

$$\dot{\boldsymbol{x}}^a(t) = \boldsymbol{u}^a(t), \qquad \dot{\boldsymbol{x}}^b(t) = \boldsymbol{u}^b(t), \tag{2}$$

the control inputs satisfy $\boldsymbol{u}_{\min} \le \boldsymbol{u}^a(t), \boldsymbol{u}^b(t) \le \boldsymbol{u}_{\max}$.

Each UAV $i \in \mathcal{V}$ senses the environment within a circular region $\mathcal{C}_i^a(x_i^a(t), r_s)$ of radius $r_s \in \mathbb{R}_{>0}$, with the sensing strength decreasing with distance:

$$f_i(q, x_i^a(t)) = \begin{cases} \beta e^{-\lambda\|q - x_i^a(t)\|^2} - \gamma, & \|q - x_i^a(t)\| \le r_s, \\ 0, & \|q - x_i^a(t)\| > r_s, \end{cases}$$

where $\gamma = \beta e^{-\lambda r_s^2}$ ensures boundary continuity, $\beta \in (0,1)$ and $\lambda \in \mathbb{R}_{>0}$. Two UAVs can communicate if $\|x_i^a(t) - x_j^a(t)\| \le r_c$, where $r_c \in \mathbb{R}_{>0}$.

2.2 Control Barrier Functions

Consider a nonlinear control-affine system:

$$\dot{\boldsymbol{x}} = f(\boldsymbol{x}) + g(\boldsymbol{x})\boldsymbol{u}, \tag{3}$$

where $\boldsymbol{x} \in \mathcal{X} \in \mathbb{R}^n$ and $\boldsymbol{u} \in \mathcal{U} \in \mathbb{R}^m$. The functions $f\colon \mathbb{R}^n \to \mathbb{R}^n$ and $g\colon \mathbb{R}^n \to \mathbb{R}^{n\times m}$ are locally Lipschitz continuous. Given a safe set $\mathcal{C}(t) := \{\boldsymbol{x} \in \mathbb{R}^n \mid b(\boldsymbol{x}, t) \ge 0\}$ defined by a continuously differentiable function $b(\boldsymbol{x}, t)\colon \mathbb{R}^n \to \mathbb{R}$, the objective of a control barrier function (CBF) is to ensure the forward invariance of the safe set by appropriately designing the control input $\boldsymbol{u}$.

Definition 1. (Forward Invariance). A set $\mathcal{C}(t)$ is said to be forward invariant under a control input $\boldsymbol{u}$ if, for any initial condition $\boldsymbol{x}(t_0) \in \mathcal{C}(t_0)$, there exists a continuous trajectory $\boldsymbol{x}(t)$ such that $\boldsymbol{x}(t) \in \mathcal{C}(t)$ for all $t \in [t_0, t_1]$.

Definition 2. (Control Barrier Function). A continuously differentiable function $b(\boldsymbol{x}, t)$ is CBF for system (3) if there exists an extended class $\mathcal{K}_\infty$ function α such that, for all $t \in [t_0, t_1], \boldsymbol{x}(t) \in \mathcal{C}(t)$, the following condition holds:

$$\sup_{\boldsymbol{u}\in\mathcal{U}} \left[L_f b(\boldsymbol{x}, t) + L_g b(\boldsymbol{x}, t)\boldsymbol{u} + \frac{\partial b(\boldsymbol{x}, t)}{\partial t} + \alpha(b(\boldsymbol{x}, t)) \right] \ge 0,$$

where $L_f b(\boldsymbol{x}, t) = \frac{\partial b(\boldsymbol{x}, t)}{\partial \boldsymbol{x}} f(\boldsymbol{x})$ and $L_g b(\boldsymbol{x}, t) = \frac{\partial b(\boldsymbol{x}, t)}{\partial \boldsymbol{x}} g(\boldsymbol{x})$ denote the Lie derivatives of b along f and g, respectively.

Lemma 1. (Ames et al. (2017)). If $b(\boldsymbol{x}, t)$ is a time-varying CBF, then any controller $\boldsymbol{u} \in K_{cbf}(\boldsymbol{x}) := \{\boldsymbol{u} \in \mathcal{U}\colon L_f b + L_g b\boldsymbol{u} + \frac{\partial b}{\partial t} + \alpha b \ge 0\}$, ensures the forward invariance of $\mathcal{C}(t)$, and guarantees the safety of the system (3).

2.3 Spatial Aggregation Signal Temporal Logic

SaSTL extends STL by incorporating spatial aggregation and counting operators to specify both temporal and spatial properties of multi-agent systems. A predicate μ is defined by a predicate function $h(y(t, z)) : \mathbb{R}^n \to \mathbb{R}$ as

$$\mu := \begin{cases} \text{True}, & h(y(t, z)) \ge 0, \\ \text{False}, & h(y(t, z)) < 0, \end{cases} \tag{4}$$

where z is the spatial location. The syntax of SaSTL is

$$\varphi ::= \mu \mid \neg\varphi \mid \varphi_1 \wedge \varphi_2 \mid \varphi_1 U_{[t_a,t_b]} \varphi_2 \mid \mathcal{A}_{\mathcal{D}}^{\text{op}} y \sim c \mid C_{\mathcal{D}}^{\text{op}} \varphi \sim c,$$

where $\text{op} \in \{\min, \max, \text{sum}, \text{avg}\}$, $\sim \in \{<, \le, =, >, \ge\}$, and $c \in \mathbb{R}$. The temporal operators $F_{[t_a,t_b]}$ and $G_{[t_a,t_b]}$ denote *Eventually* and *Always*, respectively.

Spatial relations are modeled by an undirected weighted graph $\mathcal{G} = (Z, \mathcal{E}, w)$, where Z is the set of spatial locations, $\mathcal{E}$ is the edge set, and w defines pairwise distances. The spatial domain is defined as $\mathcal{D} := ([d_1, d_2], \tau)$, where $[d_1, d_2]$ specifies the spatial interval and τ encodes spatial propositions. For a location $z \in Z$, the neighboring set satisfying $\mathcal{D}$ is $Z_{\mathcal{D}}^z := \{z' \in Z \mid d_1 \le w(z, z') \le d_2,\ z' \models \tau\}$. The corresponding signal values are collected as $\varpi_{\mathcal{D}}(y, t, z) = \bigcup_{z'\in Z_{\mathcal{D}}^z} \{y(t, z')\}$. Then, $\mathcal{A}_{\mathcal{D}}^{\text{op}} y \sim c$ evaluates aggregated signal values over $\varpi_{\mathcal{D}}$, while $C_{\mathcal{D}}^{\text{op}} \varphi \sim c$ quantifies the number or ratio of locations satisfying φ. Specifically, $C_{\mathcal{D}}^{\text{op}} \varphi = \text{op}(\{\vartheta((y, t, z') \models \varphi) \mid z' \in Z_{\mathcal{D}}^z\})$, where $\vartheta((y, t, z) \models \varphi) = 1$ if $(y, t, z) \models \varphi$, and $\vartheta((y, t, z) \models \varphi) = 0$ otherwise.

Let $(y, t, z) \models \varphi$ denote that signal y satisfies φ at time t and location z. The semantics are recursively defined as

$$(y, t, z) \models \mu \Leftrightarrow h(y(t, z)) \ge 0$$
$$(y, t, z) \models F_{[t_a,t_b]}\varphi \Leftrightarrow \exists t' \in [t + t_a, t + t_b], (y, t', z) \models \varphi$$
$$(y, t, z) \models G_{[t_a,t_b]}\varphi \Leftrightarrow \forall t' \in [t + t_a, t + t_b], (y, t', z) \models \varphi$$
$$(y, t, z) \models \mathcal{A}_{\mathcal{D}}^{\text{op}} y \sim c \Leftrightarrow \text{op}(\varpi_{\mathcal{D}}(y, t, z)) \sim c$$
$$(y, t, z) \models C_{\mathcal{D}}^{\text{op}} \varphi \sim c \Leftrightarrow \text{op}(\vartheta((y, t, z') \models \varphi) \mid z' \in Z_{\mathcal{D}}^z) \sim c$$

Robustness semantics $\rho(y, t, z, \varphi)$ quantifies the satisfaction degree of φ. Temporal operators use sup and inf in time intervals, while spatial operators evaluate robustness by aggregation over neighboring locations.

3. HIERARCHICAL UAV–UGV FRAMEWORK

3.1 Problem Formulation

We consider n UAVs operating in $\mathcal{K}$ and n UGVs moving on $\mathcal{Q}$. UAVs perform coverage and monitoring, while UGVs execute path planning with obstacle avoidance. UAVs transmit target and obstacle information to UGVs, which then plan paths under SaSTL-based CBF constraints. All tasks are monitored using SaSTL specifications, enabling real-time detection of violations and adaptive responses such as path adjustment or action rejection.

(1) **Coverage–monitoring layer:**
   (a) *Coverage:* Each UAV $i \in \mathcal{V}$ moves to a designated target position $\boldsymbol{p}^* = (p_1^*, \dots, p_n^*)^\top \in \mathbb{R}^{3\times n}$ before time t_c. The corresponding ground projection $\boldsymbol{x}^* = (x_1^*, \dots, x_n^*)^\top \in \mathbb{R}^{2\times n}$ is determined such that the sensing impact over $\mathcal{Q}$ is maximized. During this process, UAVs detect both signal distribution g_i^s and obstacle information $\mathcal{C}_i^o$.
   (b) *Monitoring:* UAVs employ SaSTL semantics to monitor both their coverage performance and the UGVs' execution of path planning and obstacle avoidance. The mission is regarded as unsuccessful if any UAV fails to satisfy the coverage specification, or if any UGV collides with an obstacle or fails to reach its assigned target.

(2) **Planning–avoidance layer:** The UGVs must reach their target positions $\boldsymbol{x}^*$ before t_f, to eliminate signal impacts, and avoid obstacles $\bigcup_{i\in\mathcal{O}} \mathcal{C}_i^o$. This is formulated using timed reach-avoid formulas, which are a subset of SaSTL. Only safety and reachability behaviors are explicitly considered in this work, whereas the specific process of signal elimination is omitted.

Our objective is to design control laws to optimize the following cost functions under safety and input constraints:

$$\mathcal{H}(\boldsymbol{x^a}(t), \mathcal{Q}) = \max \int_{\mathcal{Q}} f_i(q, x_i^a(t))\phi(q)dq, \tag{5a}$$

$$J(\boldsymbol{u}^b(t)) = \min_{\boldsymbol{u}^b} \int_{t_c}^{t_f} \boldsymbol{u}^{b^T} P \boldsymbol{u^b}, \tag{5b}$$

$$\text{s.t.} \quad \boldsymbol{p}(t) \in \mathcal{K}, \boldsymbol{x}^a(t) \in \mathcal{Q}, \boldsymbol{x}^b(t) \in \mathcal{Q} \backslash \bigcup\nolimits_{i\in\mathcal{O}} \mathcal{C}_i^o \tag{5c}$$

$$\boldsymbol{u}^a(t), \boldsymbol{u}^b(t) \in \mathcal{U}, \Delta\boldsymbol{u}^a(t), \Delta\boldsymbol{u}^b(t) \in \Delta\mathcal{U} \tag{5d}$$

where P is a positive definite matrix. Equation (5a) represents the coverage objective, which maximizes the sensing impact on $\mathcal{Q}$. Equation (5b) specifies the path planning objective for UGVs with quadratic costs. Constraint (5c) enforces feasible states within the operational environment and ensures obstacle avoidance, while constraint (5d) describes the admissible inputs and their variations.

3.2 Coverage Control

The coverage objective (5a) aims to maximize the impact on $\mathcal{Q}$. A widely adopted approach employs Voronoi tessellation Cortes et al. (2004), which divides the environment into disjoint regions assigned to each UAV. Specifically, each UAV computes the optimal point of the Voronoi cell based on its position, neighboring positions, and sensing radius. The Voronoi tessellation of UAV i is given by $V_i(x_i^a(t)) = \{q \in \mathcal{Q} \mid \|q - x_i^a(t)\| \le \|q - x_j^a(t)\|, \forall j \neq i\}$.

Accordingly, (5a) can be reformulated as

$$\mathcal{H}(\boldsymbol{x}^a(t), \boldsymbol{V}(t)) = \sum\nolimits_{i\in\mathcal{V}} \int_{V_i(x_i^a(t))} f_i(q, x_i^a(t))\phi(q)dq, \tag{6}$$

where $\boldsymbol{V}(t) = (V_1(x_1^a(t)), \dots, V_n(x_n^a(t)))^\top$. Following a gradient-based optimization method, the derivative of $\mathcal{H}$ with respect to $x_i^a(t)$ can be expressed as

$$\frac{\partial \mathcal{H}}{\partial x_i^a} = \int_{V_i(t)} \frac{\partial f_i(q, x_i^a(t))}{\partial x_i^a(t)} \phi(q,t)dq = M_{V_i}(x_i^a(t) - c_{V_i}(t)),$$

where $M_{V_i}(t)$ and $c_{V_i}(t)$ denote the mass and centroid of the Voronoi cell $V_i(t)$, respectively:

$$M_{V_i}(t) = \int_{V_i(t)} 2\beta\lambda e^{-\lambda\|q - x_i^a(t)\|^2} \phi(q)\, dq, \tag{7a}$$

$$c_{V_i}(t) = \frac{\int_{V_i(t)} 2\beta\lambda e^{-\lambda\|q - x_i^a(t)\|^2} \phi(q) q\, dq}{M_{V_i}(t)}. \tag{7b}$$

Thus, the control law for each UAV i is designed as

$$u_i^a(t) = -\kappa_a(x_i^a(t) - c_{V_i}(t)), \tag{8}$$

where $\kappa_a > 0$ is a control gain.

Theorem 1. Consider a swarm $\mathcal{V}$ of n UAVs governed by the control law (8). Then, each UAV $i \in \mathcal{V}$ asymptotically converges to the centroid $c_{V_i} = x_i^*$ of its Voronoi cell V_i.

Proof. Define a Lyapunov candidate function as $V(t) = \frac{1}{2}\sum_{i\in\mathcal{V}} \|x_i^a(t) - c_{V_i}(t)\|^2$. Taking its time derivative along trajectories yields $\dot{V}(t) = \sum_{i\in\mathcal{V}} (x_i^a(t) - c_{V_i}(t))^T \dot{x}_i^a(t)$. Substituting $\dot{x}_i^a(t) = u_i^a(t) = -\kappa_a(x_i^a(t) - c_{V_i}(t))$, we get

$$\dot{V}(t) = -\kappa_a \sum\nolimits_{i\in\mathcal{V}} \|x_i^a(t) - c_{V_i}(t)\|^2 \le 0, \tag{9}$$

which implies that $V(t)$ is non-increasing. By LaSalle's invariance principle, the trajectories converge to the largest invariant set satisfying $\dot{V}(t) = 0$, i.e., where $x_i^a(t) = c_{V_i}(t)$ for all $i \in \mathcal{V}$. Hence, each UAV asymptotically converges to the centroid of its Voronoi cell. ■

3.3 Monitoring with SaSTL

To formally specify the monitoring tasks, we employ SaSTL formulas defined as follows:

$$\psi ::= \text{True} \mid \mu \mid \neg\mu \mid \psi_1 \wedge \psi_2, \tag{10a}$$

$$\varphi ::= F_{[a,b]}\psi \mid G_{[a,b]}\psi \mid \psi_1 U_{[a,b]}\psi_2 \mid \mathcal{A}_{\mathcal{D}}^{\text{op}} y \sim c \mid C_{\mathcal{D}}^{\text{op}}\varphi \sim c \mid \varphi_1 \wedge \varphi_2, \tag{10b}$$

where ψ denotes the non-temporal formula, and φ is the temporal formula. The objective in (5) can be encoded as a monitoring specification under SaSTL semantics:

$$\varphi_1 := F_{[t_0:t_c]}\mathcal{A}^{\min}_{([0,r_s],\mathcal{S})}\|x_i^s - x_j^a\| \le 3\sigma_i, \tag{11a}$$

$$\varphi_2 := C^{\min}_{([0,\infty),\mathcal{V})}\big(F_{[t_0:t_c]}(\|x_i^a - c_{V_i}\| \le \varepsilon)\big) = 1, \tag{11b}$$

$$\varphi_3 := G_{[t_c:t_f]}(\|\boldsymbol{x}^b - \boldsymbol{x}^o\| \ge r_o), \tag{11c}$$

$$\varphi_4 := F_{[t_c:t_f]}(\|\boldsymbol{x}^b - \boldsymbol{x}^*\| \le \varepsilon), \tag{11d}$$

where the range of $3\sigma_i$ is generally considered the main distribution region of signal i, implying that 99.7% of the signal is concentrated within a radius of 3σ. Equations (11a-11b) specify UAV-related coverage objectives:

(1) each signal is covered by at least one UAV;
(2) each UAV converges to its Voronoi centroid.

In particular, φ_1 requires that, for every signal i, there exists at least one UAV j within distance $3\sigma_i$ during

the interval $[t_0, t_c]$. The formula φ_2 ensures that each UAV eventually converges to its Voronoi centroid c_{V_i} and remains within an ε-neighborhood, where $\varepsilon > 0$ is the error bound. Equations (11c-11d) define the UGV-level tasks. Formula φ_3 enforces obstacle avoidance by requiring UGV–obstacle distance to remain greater than r_o during $[t_c, t_f]$. Formula φ_4 guarantees that each UGV eventually reaches its designated target $\boldsymbol{x}^*$ within $[t_c, t_f]$ and subsequently remains within an ε-neighborhood.

The detailed monitoring process is summarized in *Algorithm 1*, which evaluates each requirement φ_1–φ_4, respectively. The distributed parallel search algorithm `deScan()` is adopted to identify locations satisfying $\mathcal{D}$.

Algorithm 1 SaSTL Monitoring Algorithm

Input: Signals $g_i^s(q, \sigma_i, x_i^s)$, time interval $[t_0, t_f]$, locations (x_i^a, x_i^b, x^o, x^*), parameters r_s, r_o, ε, graph $\mathcal{G}$
Output: Satisfaction values $\rho_{\varphi_1}, \rho_{\varphi_2}, \rho_{\varphi_3}, \rho_{\varphi_4}$
begin
  $\rho_{\varphi_1} \leftarrow -\infty$;
  for $t \in [t_0 : t_c]$ **do**
    $\varrho := 0$, $v := +\infty$;
    $Z^{x_i^s}_{[0,r_s],\mathcal{S}} := \texttt{deScan}(x_i^s, \mathcal{G}, ([0, r_s], \mathcal{S}))$;
    for $x_j^a \in Z^{x_i^s}_{[0,r_s],\mathcal{S}}$ **do**
      $v := \min(v, \|x_i^s(t) - x_j^a(t)\|)$, $\varrho := \varrho + 1$;
    if $\varrho == 0$ **then return** $\rho_t \leftarrow -\infty$;
    else return $\rho_t \leftarrow r_s - v$;
    $\rho_{\varphi_1} \leftarrow \max(\rho_{\varphi_1}, \rho_t)$;
  $\rho_{\varphi_2} \leftarrow -\infty$;
  for $t \in [t_0 : t_c]$ **do**
    $\varrho := 0$, $E :=$ EmptyList();
    $Z^{x_i^a}_{[0,\infty],\mathcal{V}} := \texttt{deScan}(x_i^a, \mathcal{G}, ([0, \infty], \mathcal{V}))$;
    for $c_{V_i} \in Z^{x_i^a}_{[0,\infty],\mathcal{V}}$ **do**
      $\rho_t \leftarrow \varepsilon - \|x_i^a(t) - c_{V_i}(t)\|$, E.add($\rho_t$);
      $\varrho \leftarrow \varrho + 1$;
    if $\varrho == 0$ **then return** $\rho_t \leftarrow -\infty$;
    else return $\rho_t \leftarrow E$.min();
    $\rho_{\varphi_2} \leftarrow \max(\rho_{\varphi_2}, \rho_t)$;
  $\rho_{\varphi_3} \leftarrow +\infty$;
  for $t \in [t_c : t_f]$ **do**
    $\rho_t \leftarrow \|x^b(t) - x^o(t)\| - r_o$; $\rho_{\varphi_3} \leftarrow \min(\rho_{\varphi_3}, \rho_t)$;
  $\rho_{\varphi_4} \leftarrow -\infty$;
  for $t \in [t_c : t_f]$ **do**
    $\rho_t \leftarrow \varepsilon - \|x^b(t) - x^*(t)\|$; $\rho_{\varphi_4} \leftarrow \max(\rho_{\varphi_4}, \rho_t)$;
  return $(\rho_{\varphi_1}, \rho_{\varphi_2}, \rho_{\varphi_3}, \rho_{\varphi_4})$;

3.4 Path Planning with Obstacle Avoidance

Motivated by Zhang et al. (2025), the *Eventually* specification φ_4 is incorporated into the objective function (5b) through an APF, while the *Always* specification φ_3 is enforced as a hard constraint by a CBF.

Consider an *Eventually* formula $\varphi_F = F_{[t_a,t_b]}\psi$, where the robustness measure of the atomic formula ψ is defined as $\rho(\boldsymbol{x}^b, t, \psi) = h(\boldsymbol{x}^b(t))$, and the cumulative robustness of φ_F is given by $\rho(\boldsymbol{x}^b, t, \varphi_F) = \sum_{t' \in [t_a,t_b]} \rho(\boldsymbol{x}^b, t + t', \psi)$. For real-time feedback controller design, $\rho(\boldsymbol{x}^b, t, \psi)$ is employed as the optimization objective, enabling the optimal control satisfying φ_F to be obtained by gradient descent. Task satisfaction is enforced by the APF formulation as follows:

$$A_{\varphi_F}(\boldsymbol{x}^b, t) = \frac{1}{2}\kappa_f \parallel \rho(\boldsymbol{x}^b, t, \text{True}) - \rho(\boldsymbol{x}^b, t, \psi) \parallel^2, \quad (12)$$

where $\kappa_f > 0$. The gradient with respect to $\rho(\boldsymbol{x}^b, t, \psi)$ is

$$\nabla A_{\varphi_F} = \frac{\partial A_{\varphi_F}(\boldsymbol{x}^b, t)}{\partial \rho(\boldsymbol{x}^b, t, \psi)} = \kappa_f \|\rho(\boldsymbol{x}^b, t, \text{True}) - \rho(\boldsymbol{x}^b, t, \psi)\|.$$

Since $\nabla A_{\varphi_F}(\boldsymbol{x}^b, t)$ decreases along trajectories satisfying $\mu = \text{True}$, it can be integrated in the objective of the path planning problem. Moreover, the *Eventually* specification φ_4 can be decomposed into n atomic formulas as

$$\begin{aligned}\varphi_4 &:= F_{[t_c:t_f]}(\|\boldsymbol{x}^b - \boldsymbol{x}^*\| \le \varepsilon) \\ &:= \bigcap_{i\in\mathcal{R}} F_{[t_c:t_f]}(\|x_i^b - x_i^*\| \le \varepsilon) = \bigcap_{i\in\mathcal{R}} \varphi_4^i. \end{aligned} \quad (13)$$

Accordingly, the objective function (5b) is reformulated as

$$J^*(\boldsymbol{u}^b, \boldsymbol{x}^b) = \min \boldsymbol{u}^{b^T} P \boldsymbol{u}^b + \sum\nolimits_{i\in\mathcal{R}} \nabla A_{\varphi_4^i}(x_i^b, t). \quad (14)$$

With multiple obstacles, the *Always* specification φ_3 is encoded via a CBF as a conjunction of atomic formulas:

$$\varphi_3 = \bigwedge_{l=1}^{k} \varphi_G^l, \quad \varphi_G^l := G_{[t_a,t_b]}\psi^l. \quad (15)$$

For each φ_G^l, a candidate CBF is defined as $b_l(\boldsymbol{x}^b, t) = h_l(\boldsymbol{x}^b(t))$ through the robustness of ψ^l, such that $b_l(\boldsymbol{x}^b, t) \ge \rho(\boldsymbol{x}^b, t, \psi^l), \forall t' \in [t + t_a, t + t_b]$. If $b_l(\boldsymbol{x}^b, t) \ge 0$ holds for all $t \ge 0$, then $(\boldsymbol{x}^b, t) \models \varphi_G^l$ is satisfied. To handle the conjunction of *Always* operators, the minimum of $h_l(\boldsymbol{x}^b(t))$ is approximated Lindemann and Dimarogonas (2019) as

$$\hat{h}(\boldsymbol{x}^b(t)) := -\frac{1}{\eta}\ln(\sum_{l=1}^{k} \exp(-\eta h_l(\boldsymbol{x}^b(t)))), \eta > 0, \quad (16)$$

which provides a smooth under-approximation of the minimum function, i.e., $\hat{h}(\boldsymbol{x}^b(t)) \le \min h_l(\boldsymbol{x}^b(t))$. According to this, a composite CBF is constructed as

$$b(\boldsymbol{x}^b, t) = -\frac{1}{\eta}\ln(\sum_{l=1}^{k} \exp(-\eta b_l(\boldsymbol{x}^b, t))). \quad (17)$$

The CBF constraint in *Definition 2* is then expressed as

$$\frac{\partial b}{\partial \boldsymbol{x}^b}(f(\boldsymbol{x}^b) + g(\boldsymbol{x}^b)\boldsymbol{u}^b) + \frac{\partial b}{\partial t} \ge -\alpha b. \quad (18)$$

Combining (14) and (18), the path planning problem is reformulated as the following QP:

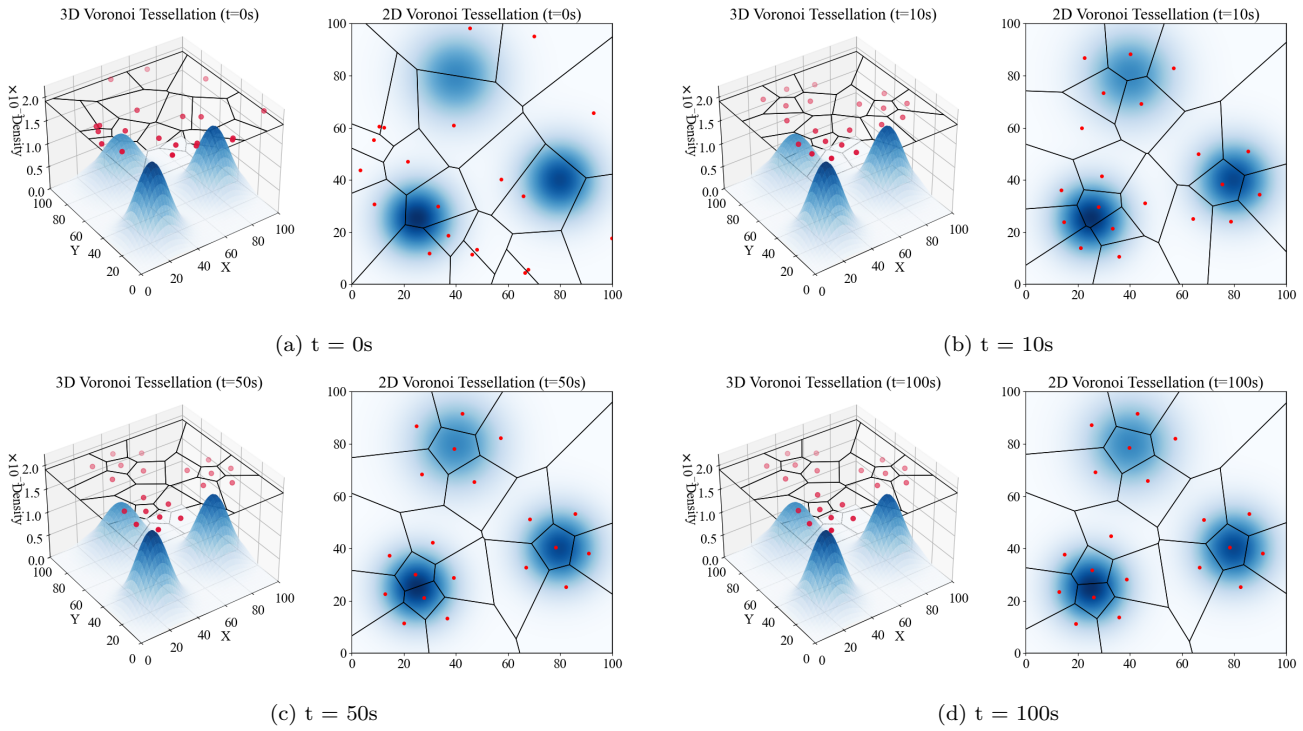
$$J(\boldsymbol{u}^b, \boldsymbol{x}^b, \delta) = \min_{\boldsymbol{u}^b, \delta} \boldsymbol{u}^{b^T} P \boldsymbol{u}^b + \sum\nolimits_{i\in\mathcal{R}} \nabla A_{\varphi_4^i}(x_i^b, t),$$

$$\text{s.t. } \frac{\partial b(\boldsymbol{x}^b, t)}{\partial \boldsymbol{x}^b}\big(f(\boldsymbol{x}^b) + g(\boldsymbol{x}^b)\boldsymbol{u}^b\big) + \frac{\partial b(\boldsymbol{x}^b, t)}{\partial t} \ge -\alpha(b(\boldsymbol{x}^b, t)).$$

When the APF-driven objective directs the agent toward an obstacle (a conflict), the QP solver prioritizes the CBF constraint. The agent will follow the safe set's boundary, effectively bypassing the obstacle while maintaining the minimum possible deviation from the APF's intended path. This mitigates conservativeness and provides a robust between task progress and collision avoidance.

4. NUMERICAL SIMULATIONS

Consider $\mathcal{K}$ and $\mathcal{Q}$ containing 20 UAVs and UGVs, with side length 100 m. There exists 3 signals located at $x_1^s = [25, 25]$, $x_2^s = [80, 40]$, and $x_3^s = [40, 80]$, with $\sigma_1^2 = 100$,



(a) t = 0s (b) t = 10s

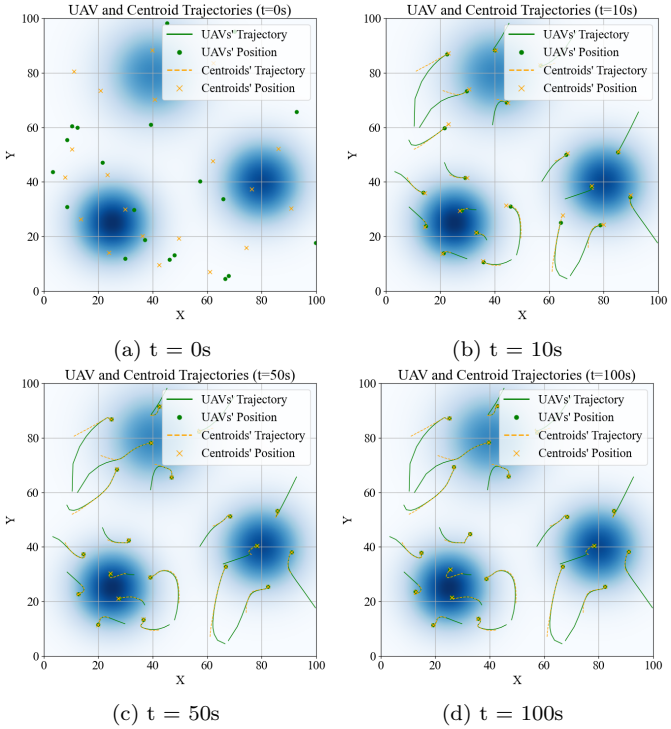
(c) t = 50s (d) t = 100s

Fig. 1. UAV coverage trajectories under the Voronoi-based control law with different time instants.

$\sigma_2^2 = 110$, and $\sigma_3^2 = 150$, respectively. The parameters of UAV are $r_c = 20$ m, $r_s = 50$ m, $\beta = 1$ and $\lambda = 0.02$. The control gains are $\kappa_a = 0.6$, $\kappa_f = 2$, and error bound is $\varepsilon = 0.15$ m. The coverage task must be completed within $t_c = 100$ s, and the path planning task within $t_f = 200$ s.

The UAV coverage results are shown in Figs. 1 and 2. Initially, the UAVs are randomly distributed in $\mathcal{K}$, and each UAV constructs a Voronoi tessellation, as shown in Fig. 1(a). At this stage, some UAVs do not cover any signal, and their positions do not coincide with the centroids of the corresponding Voronoi cells, as illustrated in Fig. 2(a), where green circles and yellow crosses denote UAVs and Voronoi centroids, respectively. After the coverage control algorithm is activated, the UAVs gradually converge to the centroids of their Voronoi cells, while the Voronoi tessellations evolve dynamically, as shown in Figs. 1(b)–(c) and Figs. 2(b)–(c). The green solid and yellow dotted lines represent the trajectories of UAVs and centroids, respectively. At $t = 50$ s, all UAVs successfully cover the signals within the corresponding 3σ regions. The coverage state at $t = 100$ s remains nearly unchanged, indicating convergence and successful completion of the coverage task. These results demonstrate that the proposed control law effectively maximizes the coverage performance and achieves the objective in (5a).

After completing the coverage task, the UAVs transmit the environmental information at $t = 100$ s to the UGVs, including the final projected positions x^*, Voronoi centroids c_{V_i}, and obstacle information $\mathcal{C}_i^o$, as shown in Fig. 3(a). Based on this information, the UGVs perform obstacle-aware path planning, as illustrated in Fig. 3(b). Three circular obstacles with radius $r_o = 5$ m are considered, and all UGVs are initialized at $[80, 0]$, representing a rescue center or base station. Each UGV then moves toward its



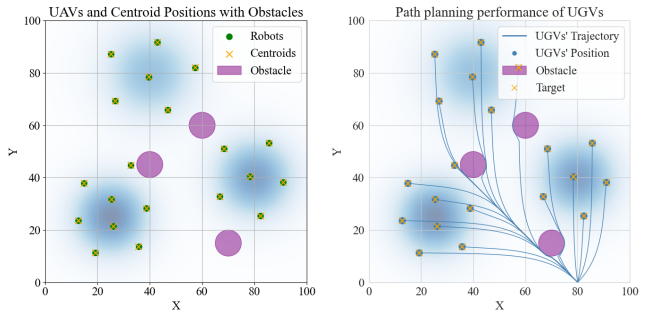
(a) t = 0s (b) t = 10s

(c) t = 50s (d) t = 100s

Fig. 2. UAV and Centroid Trajectories.

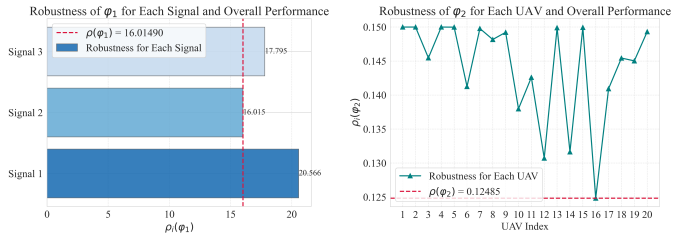
assigned target along a feasible shortest path by solving the optimal control problem with CBF constraints. The results show that all UGVs successfully reach their targets while avoiding collisions and satisfying safety constraints.

To evaluate the proposed SaSTL-based monitoring scheme, the robustness degrees of formulas φ_1–φ_4 are computed throughout the simulation by *Algorithm 1*. Fig. 4 presents the robustness values for 20 UAV coverage tasks and 20

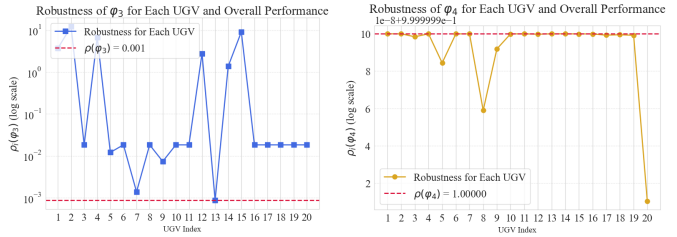


(a) Environmental information (b) UGV path planning results

Fig. 3. Environment and UGV planning results.



(a) φ_1: Signal coverage (b) φ_2: UAV convergence



(c) φ_3: Obstacle avoidance (d) φ_4: Target reaching

Fig. 4. Evaluation of SaSTL robustness for UAV and UGV.

UGV planning tasks, where Figs. 4(a)–(d) correspond to signal coverage, UAV convergence to Voronoi centroids, UGV obstacle avoidance, and successful arrival at $\boldsymbol{x}^*$ before t_f, respectively. All robustness values remain positive, indicating that all specifications are satisfied and demonstrating the effectiveness of the monitoring approach.

5. CONCLUSION

This paper proposed a two-layer UAV–UGV cooperative framework under SaSTL specifications, where UAVs perform aerial coverage and environmental monitoring, while UGVs execute obstacle-aware path planning. By decomposing spatial–temporal specifications into *Eventually* and *Always* fragments, the framework combines APF and CBFs to ensure real-time task satisfaction and safety. In addition, the SaSTL-based monitoring mechanism provides quantitative evaluation of system performance and specification satisfaction. Numerical simulations verified the effectiveness of the proposed approach in achieving robust UAV–UGV cooperation. Future extensions will implement the framework on real robotic platforms.

REFERENCES

Ames, A.D., Xu, X., Grizzle, J.W., and Tabuada, P. (2017). Control barrier function based quadratic programs for safety critical systems. *IEEE Transactions on Automatic Control*, 62(8), 3861–3876.

Belta, C. and Sadraddini, S. (2019). Formal methods for control synthesis: An optimization perspective. *Annual Review of Cont., Robot., and Auto. Sys.*, 2(1), 115–140.

Cortes, J., Martinez, S., Karatas, T., and Bullo, F. (2004). Coverage control for mobile sensing networks. *IEEE Trans. on robotics and Automation*, 20(2), 243–255.

Haghighi, I., Mehdipour, N., Bartocci, E., and Belta, C. (2019). Control from signal temporal logic specifications with smooth cumulative quantitative semantics. In *IEEE 58th Conf. on Decision and Control*, 4361–4366.

Lindemann, L. and Dimarogonas, D.V. (2019). Control barrier functions for signal temporal logic tasks. *IEEE Control Systems Letters*, 3(1), 96–101.

Lizzio, F.F., Capello, E., and Guglieri, G. (2022). A review of consensus-based multi-agent uav implementations. *Journal of Intelligent & Robotic Systems*, 106(2), 43.

Ma, M., Bartocci, E., Lifland, E., Stankovic, J.A., and Feng, L. (2021). A novel spatial–temporal specification-based monitoring system for smart cities. *IEEE Internet of Things Journal*, 8(15), 11793–11806.

Maler, O. and Nickovic, D. (2004). Monitoring temporal properties of continuous signals. In *Intl. symp. on formal techniques in real-time and fault-tolerant sys.*, 152–166.

Palacios-Gasós, J.M., Talebpour, Z., Montijano, E., Sagüés, C., and Martinoli, A. (2017). Optimal path planning and coverage control for multi-robot persistent coverage in environments with obstacles. In *IEEE International Conf. on Robotics and Automation*, 1321–1327.

Wang, Z., Piao, S., Ji, Y., Wang, X., and Tsung, F. (2025). An efficient dual-observer method for leader-following consensus control of multiagent systems. In *IEEE 21st Intl. Conf. on Auto. Sci. and Engineering*, 3468–3473.

Yousefi, M.H., Behnam, B., and Farahani, S. (2024). An auxiliary framework to facilitate earthquake search and rescue operations in urban regions. *Natural Hazards*, 120(12), 11107–11131.

Zhang, S. and Ji, Y. (2025a). Distributed resilient consensus and demand tracking in battery energy storage systems under adversarial attacks. In *IEEE 19th International Conf. on Control and Automation*, 268–273.

Zhang, S. and Ji, Y. (2025b). Resilient consensus control with privacy protection for battery energy storage systems. *IEEE Control Systems Letters*, 9, 2133–2138.

Zhang, S., Liu, Z.W., Wen, G., and Wang, Y.W. (2024). Accelerated distributed optimization algorithm with malicious nodes. *IEEE Transactions on Network Science and Engineering*, 11(2), 2238–2248.

Zhang, Y., Jiang, T., Cai, Z., and Ji, Y. (2026). Safety-critical control under timed reach-avoid specifications: A backup control barrier function approach. *IEEE Control Systems Letters*, 10, 109 – 114.

Zhang, Y., Zhang, S., Miao, S., and Ji, Y. (2025). A task decomposition approach for signal temporal logic control. In *2025 China Auto. Congress*, 3242–3247.

Zhao, Y., Yu, X., Hoxha, B., Fainekos, G., Deshmukh, J., and Lindemann, L. (2025). STL-GO: Spatio-temporal logic with graph operators for distributed systems with multiple network topologies. *ACM Transactions on Embedded Computing Systems*, 24(5s), 1–23.

Zhong, M. and Cassandras, C.G. (2011). Distributed coverage control and data collection with mobile sensor networks. *IEEE Transactions on Automatic Control*, 56(10), 2445–2455.